applied optics

Pr^{3+}:YLF mode-locked laser at 640 nm directly pumped by InGaN-diode lasers

KODAI IIJIMA, RYOSUKE KARIYAMA, HIROKI TANAKA, AND FUMIHIKO KANNARI*

Department of Electronics and Electrical Engineering, Keio University, 3-14-1, Hiyoshi, Kohoku-ku, Yokohama 223-8522, Japan
**Corresponding author: kannari@elec.keio.ac.jp*

Received 12 July 2016; revised 21 August 2016; accepted 29 August 2016; posted 30 August 2016 (Doc. ID 270321); published 22 September 2016

We attain stable mode-locking of an InGaN laser-diode-pumped Pr^{3+}:YLF laser with a pump power of 2.8 W using a semiconductor saturable absorption mirror. A maximum averaged output power of 65 mW was obtained with a 45-ps pulse width at a pulse repetition rate of 108 MHz. We also attempted Kerr-lens mode-locking by employing an SF57 glass in a cavity as a Kerr medium.

OCIS codes: (140.3480) Lasers, diode-pumped; (140.3580) Lasers, solid-state; (140.4050) Mode-locked lasers; (140.7300) Visible lasers.

http://dx.doi.org/10.1364/AO.55.007782

1. INTRODUCTION

Coherent ultrafast pulse lasers in the visible wavelength region are useful light sources in spectroscopy, material processing, medicine, and biology. Conventionally, visible ultrafast laser pulses can be generated as a second harmonic of near-infrared laser pulses by employing frequency conversion techniques. However, ideally, we can replace them with all solid-state direct oscillating visible laser systems for improving compactness and cost effectiveness.

Trivalent praseodymium ion (Pr^{3+}) is a unique laser gain material that has many optical transitions in a wide range of the visible region from 480 to 720 nm. Because of its utilities for miniaturization or efficiency improvement, Pr^{3+}-doped laser media are gathering attention because they permit oscillation in the visible region without frequency conversion.

For room temperature operation of a Pr^{3+} laser, host materials of low phonon energy are required, and laser actions of Pr^{3+} lasers are obtained with fluoride hosts, such as YLF ($LiYF_4$) [1], LLF ($LiLuF_4$) [2], KYF(KY_3F_{10}) [3] crystals, and ZBLAN [4] and AlF_3 [5] fibers. Since Pr^{3+}-doped fluorides have absorption peaks around 440 nm, they can be pumped by InGaN blue laser diodes (LDs) whose output power and efficiency have been making significant progress [6]. In particular, a Pr^{3+}:$LiYF_4$ (YLF) laser was reported with high efficiencies (slope efficiency up to ~60%) and a low threshold [7,8]. The Pr^{3+}:YLF laser enabled direct oscillations at deep red (~720, ~700 nm), red (~640 nm), orange (~610 nm), and green (~520 nm) transitions have been realized at room temperature.

Regarding the pulsed oscillation of Pr^{3+} lasers, passive *Q*-switching was reported with a semiconductor saturable absorber mirror (SESAM) [9], Cr^{4+}:YAG crystal [10,11], gold nanoparticles [12], and nanosheets of transition metal dichalcogenides (TMDs) [13,14] as saturable absorbers. Kerr-lens mode-locking of Pr^{3+}:YLF lasers at 607 and 640 nm was realized with argon-ion laser pumping [15,16].

Recently, using a SESAM, Gaponenko *et al.* successfully demonstrated a passively mode-locked Pr^{3+}:YLF laser pumped by a frequency-doubled optically pumped semiconductor laser (2ω-OPSL) operating at the red wavelength [17]. The maximum averaged output power reached 16 mW at an incident pump power of 3.75 W with a mode-locked pulse width of 18 ps (FWHM). Due to the narrow gain bandwidth of the transition ($^3P_0 \rightarrow {}^3F_2$) in the Pr^{3+}:YLF, generating mode-locked subpicosecond pulses is challenging.

In this paper, to the best of our knowledge, we report the first SESAM mode-locked Pr^{3+}:YLF laser that is directly pumped by InGaN LDs. On the other hand, since broadband SESAMs are not available, and high-power laser operation is prohibited due to the low damage threshold of SESAMs, pure Kerr-lens mode-locking of Pr^{3+}:YLF lasers is still desired. However, for multimode diode pumping, obtaining sufficient self-focusing cannot be expected because of relatively low intracavity intensity. Moreover, multimode diode pumping tends to induce multimode laser oscillation. For solving these problems, in this work, we employed an SF57 glass as a Kerr medium and attempted a hard-aperture Kerr-lens mode-locking [18].

2. SESAM MODE-LOCKING OF Pr^{3+}:YLF LASER AT 640 NM

A. Experimental Setup

The experimental setup of a SESAM mode-locked Pr^{3+}:YLF laser is depicted in Fig. 1. A 5-mm-long Pr^{3+}:YLF crystal

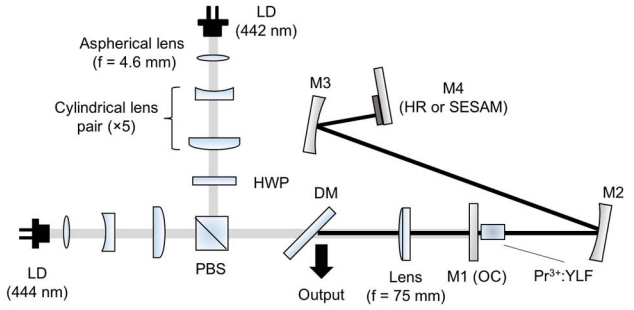

Fig. 1. Schematic view of cavity configuration for a SESAM mode-locked Pr^{3+}:YLF laser: polarization beam splitter (PBS); half-wave plate (HWP); dichroic mirror (DM); and output coupler (OC).

(Unioriental Inc.) doped with Pr^{3+} at a concentration of 0.5 at. %, which was cut parallel to the c-axis, was placed in front of the plane pumping mirror. As pump sources, we used two InGaN blue LDs (Nichia Inc.). Each output power reached 3.5 W. The LD's emitter size was 1 × 30 μm with a divergence angle of 2θ of 45.9 × 13.9°, which corresponded to M^2 = 1.5 × 13 (fast axis × slow axis). To maximize the absorbed power, the wavelength of each LD was tuned to 444 and 442 nm by Peltier devices, since the Pr^{3+}:YLF crystal respectively has absorption peaks at 444 and 442 nm for polarization parallel to the c- and a-axes [19]. The pump beam from each LD was collimated by an aspherical lens with a focal length of 4.6 mm and expanded along the slow axis by a cylindrical lens pair (f = −20 and 100 mm). Then the beam was focused into the Pr^{3+}:YLF crystal through a lens whose focal length was 75 mm. At 444 and 442 nm, the absorption coefficients of the Pr^{3+}:YLF crystal were measured to be 3.54 and 1.16/cm, which respectively corresponded to absorbed pump powers of 2.2 and 1.6 W. Therefore, the total absorbed pump power reached 3.8 W.

The SESAM in this experiment contained three 6-nm-thick GaInP quantum wells that were embedded within an AlGaInP cavity and placed on top of a 40-pair AlGaAs/AlAs distributed Bragg reflector (DBR) (RefleKron Ltd.) that had a center reflection wavelength of 640 nm, a response time of 300 ps, and an unsaturated reflectivity of 97%. According to the 2ω-OPSL pumped Pr^{3+}:YLF mode-locked laser reported by Gaponenko *et al.* [17], who used the same SESAM as we used, the necessary intensity of the SESAM for achieving stable mode-locking was estimated to be ~23 MW/cm^2.

The 1.4-m-long Z-folded laser cavity consists of four mirrors: an output coupler M1 (OC) with 10% transmission; two high-reflectivity (HR) concave mirrors, M2, M3 (ROC_{M2} = 100 mm, ROC_{M3} = 75 mm); and a plane mirror M4 (HR mirror or SESAM). To obtain stable mode-locking, the SESAM intensity must be higher than the estimated saturation intensity. For designing the cavity mode of TEM_{00}, we used the cavity design proposed by Qiao *et al.* [20] to compensate for the astigmatism on the SESAM and to reach sufficiently high intracavity intensity. Equations (1) and (2) express the effective focal lengths of a concave mirror in the sagittal and tangential directions when the angle of incidence is θ [21]:

$$f_s = f/\cos\theta, \tag{1}$$

$$f_t = f \cdot \cos\theta. \tag{2}$$

When a Gaussian beam is focused by a lens with a focal length of f, Eqs. (3) and (4) provide the relationship between a spot size and a distance from the concave mirror to the spot [22]:

$$\frac{1}{w'^2_{1,2}} = \frac{1}{w^2_{1,2}}\left(1 - \frac{l_{1,2}}{f}\right) + \frac{1}{f^2}\left(\frac{\pi w_{1,2}}{\lambda}\right)^2, \tag{3}$$

$$l'_{1,2} - f = (l_{1,2} - f)\frac{f^2}{(l_{1,2} - f)^2 + \left(\frac{\pi w^2_{1,2}}{\lambda}\right)^2}, \tag{4}$$

where λ is the wavelength, w is the spot size, l is the distance from the spot to the concave mirror, the apostrophe denotes the transcribed state, and subscripts 1 and 2 represent the sagittal and tangential planes.

Using these equations, a Z-folded cavity, in which the astigmatism can be compensated at the focal spots, is designed in the following three steps: (1) set a spot size (w_1); (2) set a concave mirror (M2) at a position where the Gaussian beam radius corresponds to the beam radius after being transcribed by a concave mirror (M3) in both the sagittal and tangential planes; and (3) set an M2 angle to correspond to the transcribed spot size (w'_2) in the sagittal and tangential planes. In this experiment, we designed a cavity so that the beam waist spot size became 10 μm × 10 μm. The mode-matching efficiency between the pump and cavity modes was calculated to be 78%. With this cavity, the estimated value of the averaged output power, that we had to obtain for reaching the SESAM's saturation intensity, was 14 mW.

B. Experimental Results and Discussion

With an M4 HR mirror, we obtained an averaged CW output power of 550 mW and replaced the plane M4 mirror by a SESAM to achieve mode-locked oscillation. Figure 2 shows the output power as a function of the absorbed pump power. From an absorbed pump power of 2.8 W, stable mode-locking started. At a maximum absorbed pump power of 3.8 W, we obtained the highest averaged output power of 65 mW at a pulse repetition rate of 108.7 MHz. The mode-locked pulse

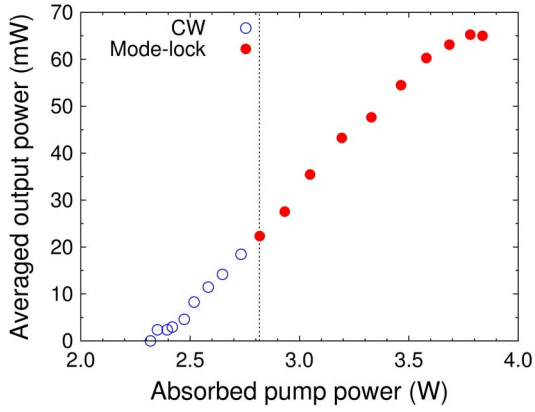

Fig. 2. Output power of SESAM mode-locked Pr^{3+}:YLF laser as function of absorbed pump power.

width was measured as 45 ps (FWHM) by a streak camera (Hamamatsu C4334, 15-ps resolution) (Fig. 3). Figure 4 shows a spectrum measured by a spectrum analyzer (ADVANTEST Q8384 Optical Spectrum Analyzer, 0.01-nm resolution) under mode-locked operation. The center wavelength was 639.7 nm, and the spectral width (FWHM) was 0.1 nm, which corresponded to a transform-limited pulse width of 4.2 ps. Gaponenko *et al.* obtained a pulse width of 18 ps (FWHM) with SESAM mode-locking [17]. The reason for such a longer pulse width far from the Fourier transform limit remains an open question. The actual spectrum width might be much narrower than our measurement where the spectrum was integrated over ~1 s by the optical spectrum analyzer. In fact, the measured spectrum shows some internal structures (Fig. 4). The stable mode-lock oscillation was maintained for more than a half hour.

3. KERR-LENS MODE-LOCKING

A. Experimental Setup

Figure 5 shows a schematic view of a Kerr-lens mode-locked Pr^{3+}:YLF laser cavity. A 4-mm-long, 0.5 at. % doped Pr^{3+}:YLF crystal was cut at a Brewster's angle of 55.5°. As a Kerr medium, we employed an SF57 glass, which had a huge nonlinear refractive index of 4.1×10^{-19} m^2/W [23]; the nonlinear refractive index of YLF was 1.4×10^{-20} m^2/W [24]. The 2-m-long cavity consists of six mirrors: a plane end mirror, M1; a pair of concave mirrors, M2, M3 ($ROC_{M2,3} = 75$ mm); two pumping concave mirrors, M4, M5 ($ROC_{M4,5} = 100$ mm); and an OC of 1.2%. We employed optical isolators to protect the LDs from any backreflected beams and unabsorbed opposite pump beams, which were polarized parallel to the c-axis of the Pr^{3+}:YLF and focused into the gain crystal by lenses with a 100-mm focal length.

In this experiment, we designed a cavity so that the mode size at the aperture changes significantly in the pulsed operation and realizes fine hard-aperture Kerr-lens mode-locking. The cavity stability depends on the two independent distances between the two pairs of concave mirrors that were placed on both sides of the Pr^{3+}:YLF rod and the SF57 glass. Since we expected to obtain the maximum mode size change at the end mirror, we calculated the change in mode radius

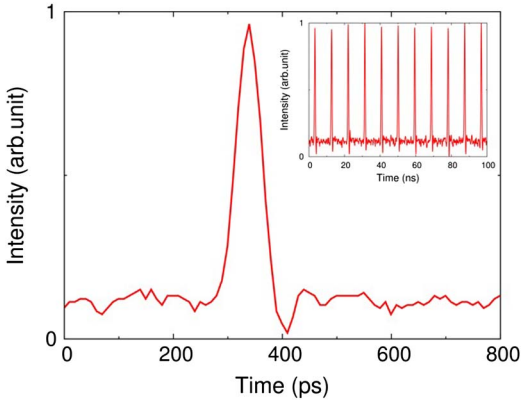

Fig. 3. Single pulse trace of SESAM mode-locked Pr^{3+}:YLF laser. Inset shows pulse train in microsecond time scale.

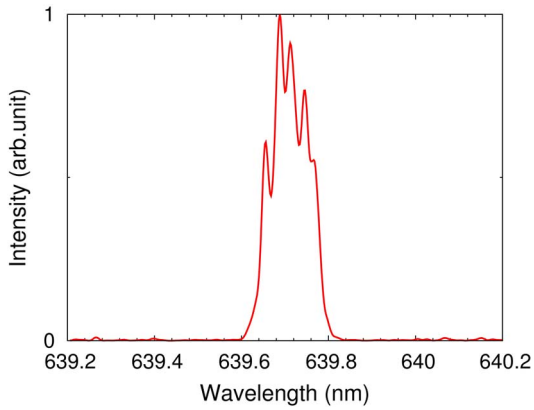

Fig. 4. Optical spectrum of a SESAM mode-locked Pr^{3+}:YLF laser measured at maximum absorbed pump power of 3.8 W. Spectral resolution was 0.01 nm.

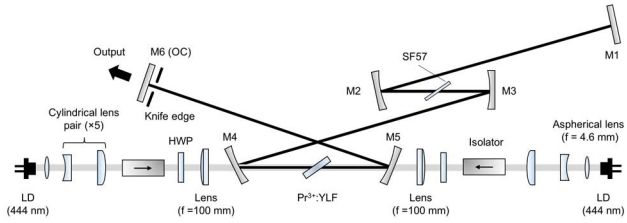

Fig. 5. Schematic view of a Kerr-lens mode-locked Pr^{3+}:YLF laser with SF57 glass.

normalized to the CW mode radius on the end mirror as the parameters of the distances between the two pairs of mirrors placed at both sides of the Pr^{3+}:YLF rod and the SF57 glass with an ABCD matrix method, based on the Kerr lens effect.

An effective focal length of the Kerr lens is given by Eq. (5):

$$\frac{1}{f_{\mathrm{Kerr}}} = \frac{4n_2PL}{w^4}. \tag{5}$$

Here, n_2 is the nonlinear refractive index, P is the peak power of the pulse incident to the Kerr medium, L is the length of the Kerr medium, and w is the beam radius. The Kerr lenses exhibiting different focal lengths f_{Kerr} are distributed in the Kerr medium. Equation (6) expresses the propagation matrix of the L long Kerr medium, which was divided into m pieces so that l $(= L/m)$ became much shorter than the Rayleigh length:

$$M_{\mathrm{slice}} = \begin{bmatrix} 1 & 0 \\ -\frac{1}{f_{\mathrm{kerr}}(w)} & 1 \end{bmatrix} \begin{bmatrix} 1 & l \\ 0 & 1 \end{bmatrix} = \begin{bmatrix} 1 & l \\ -\frac{1}{f_{\mathrm{kerr}}(w)} & 1 \end{bmatrix}. \tag{6}$$

When the beam radius is w in a l long Kerr medium, $f_{\mathrm{Kerr}}(w)$ denotes the focal length of the effective Kerr lens. The laser mode radius was assumed to be constant in each divided piece. We iteratively calculated the cavity mode based on an ABCD matrix method until the pulsed oscillation mode converged. The change in mode radius normalized to the CW mode radius at the OC is given by Eq. (7):

$$\frac{w_{\mathrm{cw}} - w_{\mathrm{pulse}}}{w_{\mathrm{cw}}}, \tag{7}$$

where w_{cw} and w_{pulse} represent the mode radius in the CW and pulsed oscillations. Because of the large beam radius in the laser crystal for our cavity design and a low nonlinear refractive index of the Pr^{3+}:YLF crystal, we did not take into account a Kerr lens effect in the laser crystal. With a pump beam radius of 61 μm × 32 μm, the mode-matching factors were estimated as 82% and 76% under CW and pulsed oscillation, respectively. Therefore, there is a little chance to realize soft-aperture Kerr-lens mode-locking with low mode-matching efficiency and the slight differences between the CW and pulsed oscillation. As a result of the mode calculation, we obtained the maximum mode radius change on the OC in the sagittal direction. Figure 6 shows the change in mode radius normalized to the CW mode radius on the OC in the sagittal direction as parameters of the distance between two concave mirrors placed on both sides of the Pr^{3+}:YLF (y-axis) and SF57 glass (x-axis), respectively. We assumed an averaged output power of 20 mW. The maximum mode radius change was estimated to be 72%, which is an upper limit that we can realize by aligning the cavity to maximize the modulation depth. However, such a large change is obtainable at very limited conditions near the boundary where the cavity becomes unstable. From the mode calculation result by an ABCD matrix, the spot size on the SF57 glass was estimated as 26 μm × 27 μm under pulsed oscillation. The averaged beam radius along the Pr^{3+}:YLF crystal was 28 μm × 45 μm.

In Fig. 7, we compared the change in the mode radius on the OC with fused silica as the nonlinear medium with that with a SF57 glass. We assumed averaged output power of 20 mW. The nonlinear refractive index of the fused silica was 2.5×10^{-20} m^2/W [25]. Since its nonlinear refractive index was much lower than that of the SF57 glass, the maximum change in a beam radius of 26% from the fused silica was smaller.

B. Experimental Results and Discussion

We obtained a CW laser power of ~1 W at a highest absorbed pump power of 4.2 W with the optimal cavity adjusted for CW operation. Figure 8 shows an output pulse train when a knife

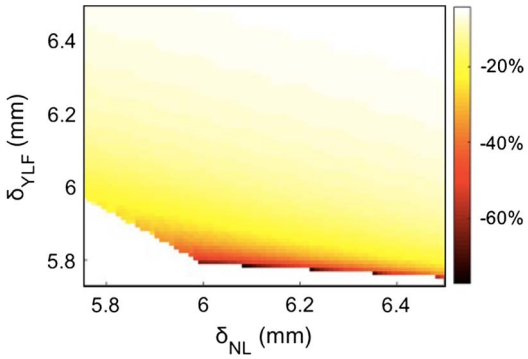

Fig. 6. The change in mode radius normalized to the CW mode radius in the sagittal direction of the end mirror with a SF57 glass. At darker range, larger beam radius change is expected. δ_{YLF} and δ_{NL} express differences from confocal length of two concave mirrors placed on both sides of Pr^{3+}:YLF and SF57 glass, respectively. Averaged output power of 20 mW was assumed with a pulse width of 15 ps.

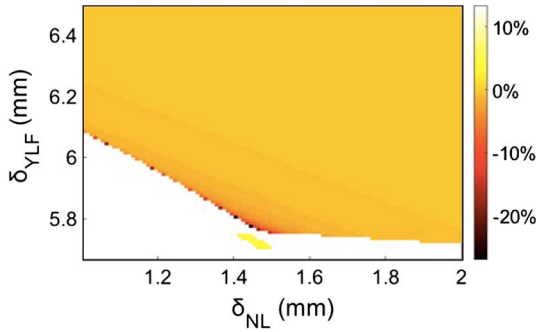

Fig. 7. Change in mode radius normalized to the CW mode radius in the sagittal direction of the end mirror with a fused silica. At darker range, larger beam radius change is expected. δ_{YLF} and δ_{NL} express differences from a confocal length of two concave mirrors placed on both sides of Pr^{3+}:YLF and fused silica, respectively. Averaged output power of 20 mW was assumed with a pulse width of 15 ps.

edge is inserted in front of the OC in the sagittal direction as well as the recorded pulse train. We observed *Q*-switch mode-locking with the averaged output power of ~50 mW. The *Q*-switched pulse repetition rate was measured as 120 kHz. The pulse width was measured as 1 ns. The pulse repetition rate was measured as 151 MHz, which is double the value calculated from a cavity length of 2 m. Presumably because the Kerr lens effect became too strong, the oscillation condition shifted to a state with a higher pulse repetition rate to reduce the pulse peak power. Then, instead of an SF57 glass, we employed fused silica to decrease the nonlinear effects. However, in this case, we failed to achieve even *Q*-switch mode-locking.

Figure 9 shows the pulse train obtained when we tapped an end mirror M1 with the SF57 glass. The pulse train, which was only measured immediately after tapping, soon switched back

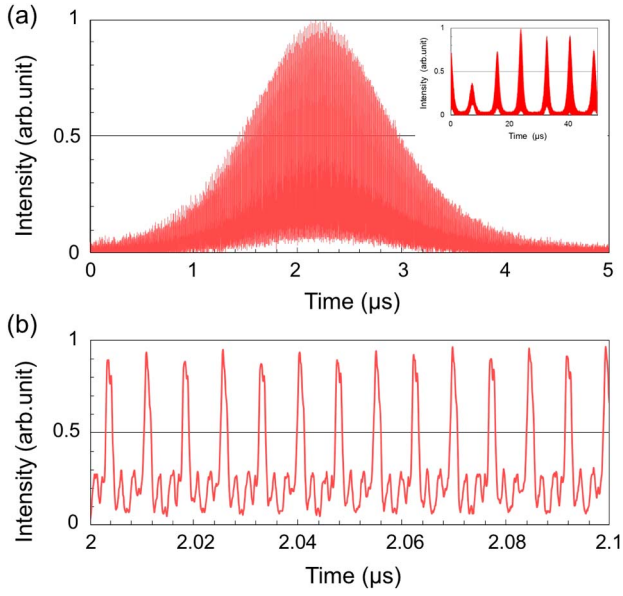

Fig. 8. (a) Output pulse of a *Q*-switch mode-locked laser in microsecond time scale. Inset shows the *Q*-switch pulse train in tens of microseconds time scale. (b) Pulse train in tens of nanoseconds time scale measured by a photodiode.

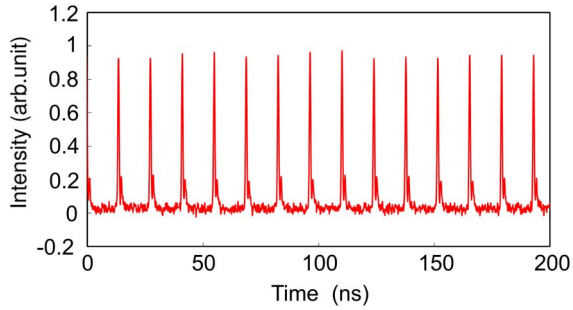

Fig. 9. Output pulse train measured only just after vibrating M6.

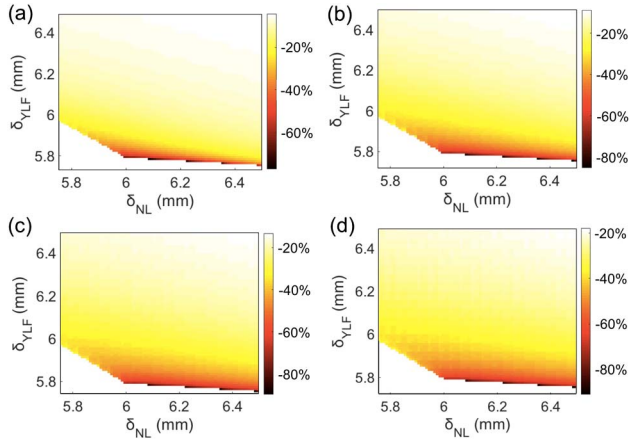

Fig. 10. Change in mode radius normalized to the CW mode radius in the sagittal direction of the end mirror when we assume 15-ps pulse width with the following averaged output power: (a) 20 mW (original condition), (b) 40 mW, (c) 60 mW, and (d) 80 mW. Scale of color bar was changed for (b), (c), and (d).

to the pulses shown in Fig. 8 within a several seconds. However, the pulse repetition rate of 75 MHz obtained by the pulse train in Fig. 9 equaled the value calculated from the cavity length. In addition, the pulse width was shortened to ~400 ps (the measurement limit value of our photodiode), which is much shorter than before tapping the mirror. These experimental results suggest that we may be able to achieve stable mode-locking at more stable cavity condition for mode-locking. Presumably, since the proper Kerr-lens mode-locking condition attained such a limited condition near the unstable cavity condition, as shown in Fig. 6, no self-sustained Kerr-lens mode-locking occurred in our cavity design.

We calculated again the beam radius reductions at the Kerr lens formation for higher intracavity laser intensities. The results are shown in Fig. 10. As the averaged output power increased from 20 to 80 mW, the cavity condition, where the beam size was reduced by more than 60%, extended to a wider area. Therefore, we may be able to attain a stable mode-lock cavity condition at high-power laser operations.

Very recently, we noticed that a thermal lens assisted KLM was achieved by Zhang *et al.* [26] with a Pr :$GdLiF_4$ laser crystal pumped by InGaN LDs in a short laser cavity. Since the Kerr nonlinearity of $GdLiF_4$ is much higher than that of YLF, this scheme will also be suitable for ultrashort pulse generation by Pr^{3+} lasers.

4. CONCLUSIONS

In this paper, to the best of our knowledge we reported the first SESAM mode-locked Pr^{3+}:YLF laser that is directly pumped by InGaN LDs. Stable mode-locked operation started from absorbed pump power of 2.8 W. At absorbed pump power of 3.8 W, a maximum averaged output power of 65 mW was obtained with a pulse width of 45 ps (FWHM) at a pulse repetition rate of 108 MHz. By employing a SF57 glass as a Kerr medium, we also tried LD-pumped Kerr-lens mode-locking. In this approach, however, we could not achieve self-sustained CW mode-locking and only obtained a *Q*-switch mode-locked pulse train whose pulse repetition rate was doubled. The laser operation only switched to CW mode-locking immediately after we tapped an end mirror. Our model calculations predicted that a stable mode-locking cavity condition could be found with larger Kerr effects at high-power laser oscillation.

Funding. Ministry of Education, Culture, Sports, Science, and Technology (MEXT), Japan; JSPS KAKENHI (24656055).

Acknowledgment. We gratefully thank Nichia Inc. for supplying the high-power InGaN blue laser diodes.

REFERENCES

1. A. Richter, E. Heumann, G. Huber, V. Ostroumov, and W. Seelert, "Power scaling of semiconductor laser pumped Praseodymium-lasers," Opt. Express **15**, 5172–5178 (2007).
2. F. Cornacchia, A. Di Lieto, M. Tonelli, A. Richter, E. Heumann, and G. Huber, "Efficient visible laser emission of GaN laser diode pumped Pr-doped fluoride scheelite crystals," Opt. Express **16**, 15932–15941 (2008).
3. P. Camy, J. L. Doualan, R. Moncorgé, J. Bengoechea, and U. Weichmann, "Diode-pumped Pr^{3+}:KY_3F_{10} red laser," Opt. Lett. **32**, 1462–1464 (2007).
4. H. Okamoto, K. Kasuga, I. Hara, and Y. Kubota, "Visible-NIR tunable Pr^{3+}-doped fiber laser pumped by a GaN laser diode," Opt. Express **17**, 20227–20232 (2009).
5. J. Nakanishi, Y. Horiuchi, T. Yamada, O. Ishii, M. Yamazaki, M. Yoshida, and Y. Fujimoto, "High-power direct green laser oscillation of 598 mW in Pr^{3+}-doped waterproof fluoroaluminate glass fiber excited by two-polarization-combined GaN laser diodes," Opt. Lett. **36**, 1836–1838 (2011).
6. S. Nakamura, M. Senoh, S. I. Nagahama, N. Iwasa, T. Yamada, T. Matsushita, H. Kiyoku, and Y. Sugimoto, "InGaN-based multi-quantum-well-structure laser diodes," Jpn. J. Appl. Phys. **35**, L74–L76 (1996).
7. A. Richter, E. Heumann, E. Osiac, G. Huber, W. Seelert, and A. Diening, "Diode pumping of a continuous-wave Pr^{3+}-doped $LiYF_4$ laser," Opt. Lett. **29**, 2638–2640 (2004).
8. P. W. Metz, F. Reichert, F. Moglia, S. Müller, D. T. Marzahl, C. Kränkel, and G. Huber, "High-power red, orange, and green Pr^{3+}:$LiYF_4$ lasers," Opt. Lett. **39**, 3193–3196 (2014).
9. S. V. Savitski, I. M. Ranieri, A. B. Krysa, and S. Calvez, "Passively Q-switched Pr:YLF laser," in *CLEO: Laser Applications to Photonic Applications*, OSA Technical Digest (CD) (Optical Society of America, 2011), paper CMB7.
10. J. Kojou, R. Abe, R. Kariyama, H. Tanaka, A. Sakurai, Y. Watanabe, and F. Kannari, "InGaN diode pumped actively Q-switched intracavity frequency doubling Pr:$LiYF_4$ 261 nm laser," Appl. Opt. **53**, 2030–2036 (2014).

11. H. Tanaka, R. Kariyama, K. Iijima, K. Hirosawa, and F. Kannari, "Saturation of 640-nm absorption in Cr^{4+}:YAG for an InGaN laser diode pumped passively *Q*-switched Pr^{3+}:YLF laser," Opt. Express **23**, 19382–19395 (2015).
12. D. Wu, J. Peng, Z. Cai, J. Weng, Z. Luo, N. Chen, and H. Xu, "Gold nanoparticles as a saturable absorber for visible 635 nm *Q*-switched pulse generation," Opt. Express **23**, 24071–24076 (2015).
13. Y. Zhang, S. Wang, H. Yu, H. Zhang, Y. Chen, L. Mei, A. Di Lieto, M. Tonelli, and J. Wang, "Atomic-layer molybdenum sulfide optical modulator for visible coherent light," Sci. Rep. **5**, 11342 (2015).
14. Y. Cheng, J. Peng, B. Xu, H. Yang, Z. Luo, H. Xu, Z. Cai, and J. Weng, "Passive *Q*-switching of a diode-pumped Pr:$LiYF_4$ visible laser using WS_2 as saturable absorber," IEEE Photon. J. **8**, 1–6 (2016).
15. S. Ruan, B. H. T. Chai, J. M. Sutherland, P. M. W. French, and J. R. Taylor, "Kerr-lens mode-locked visible transitions of a Pr:YLF laser," Opt. Lett. **20**, 1041–1043 (1995).
16. Y. P. Tong, A. V. Shestakov, B. H. T. Chai, J. M. Sutherland, P. M. W. French, and J. R. Taylor, "Self-starting Kerr-lens mode-locked femtosecond Cr^{4+}:YAG and picosecond Pr^{3+}:YLF solid-state lasers," Opt. Lett. **21**, 644–646 (1996).
17. M. Gaponenko, P. W. Metz, A. Härkönen, A. Heuer, T. Leinonen, M. Guina, T. Südmeyer, G. Huber, and C. Kränkel, "SESAM mode-locked red praseodymium laser," Opt. Lett. **39**, 6939–6941 (2014).
18. G. P. A. Malcolm and A. I. Ferguson, "Self-mode locking of a diode-pumped Nd:YLF laser," Opt. Lett. **16**, 1967–1969 (1991).
19. J. Kojou, Y. Watanabe, Y. Kojima, H. Nemoto, and F. Kannari, "Intracavity second-harmonic generation at 320 nm of an actively *Q*-switched Pr:$LiYF_4$ laser," Appl. Opt. **51**, 1382–1386 (2012).
20. W. Qiao, Z. Xiaojun, W. Yonggang, S. Liqun, and N. Hanben, "A simple method for astigmatic compensation of folded resonator without Brewster window," Opt. Express **22**, 2309–2316 (2014).
21. H. Kogelnik, E. Ippen, A. Dienes, and C. Shank, "Astigmatically compensated cavities for CW dye lasers," IEEE J. Quantum Electron. **8**, 373–379 (1972).
22. H. Kogelnik and T. Li, "Imaging of optical modes-resonators with internal lenses," Bell Syst. Tech. J. **44**, 455–494 (1965).
23. S. Friberg and P. Smith, "Nonlinear optical glasses for ultrafast optical switches," IEEE J. Quantum Electron. **23**, 2089–2094 (1987).
24. B. Braun, K. J. Weingarten, F. X. Kärtner, and U. Keller, "Continuous-wave mode-locked solid-state lasers with enhanced spatial hole burning," Appl. Phys. B **61**, 429–437 (1995).
25. R. Adair, L. L. Chase, and S. A. Payne, "Nonlinear refractive index of optical crystals," Phys. Rev. B **39**, 3337–3350 (1989).
26. Y. Zhang, H. Yu, H. Zhang, A. Di Lieto, M. Tonelli, and J. Wang, "Laser-diode pumped self-mode-locked praseodymium visible lasers with multi-gigahertz repetition rate," Opt. Lett. **41**, 2692–2695 (2016).